ACS APPLIED ELECTRONIC MATERIALS

pubs.acs.org/acsaelm Article

Classifiable Limiting Mass Change Detection in a Graphene Resonator Using Applied Machine Learning

Miri Seo,[⊥] Eunseo Yang,[⊥] Dong Hoon Shin, Yugyeong Je, Chirlmin Joo, Kookjin Lee,* and Sang Wook Lee*

Cite This: *ACS Appl. Electron. Mater.* 2022, 4, 5184−5190 Read Online

ACCESS | Metrics & More | Article Recommendations | Supporting Information

ABSTRACT: Nanomechanical resonator devices are widely used as ultrasensitive mass detectors for fundamental studies and practical applications. The resonance frequency of the resonators shifts when a mass is loaded, which is used to estimate the mass. However, the shift signal is often blurred by the thermal noise, which interferes with accurate mass detection. Here, we demonstrate the reduction of the noise interference in mass detection in suspended graphene-based nanomechanical resonators, by using applied machine learning. Featurization is divided into image and sequential datasets, and those datasets are trained and classified using 2D and 1D convolutional neural networks (CNNs). The 2D CNN learning-based classification shows a performance with f1-score over 99% when the resonance frequency shift is more than 2.5% of the amplitude of the thermal noise range.

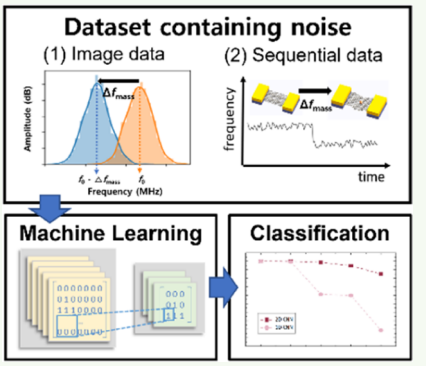

KEYWORDS: *applied machine learning, deep learning, graphene, mass detection, resonator*

INTRODUCTION

The small size, light mass, and fast switching speed make nanoelectromechanical systems (NEMS) attractive in research and applications.[1] Among NEMS devices, nanomechanical resonator devices are being used in a wide range of research fields—from fundamental physics for studying quantum mechanical limits[2−6] to practical applications such as the ultrasensitive mass detection and single molecule biosensing.[7−10] A simple spring model is used to describe the mechanism of mass detection using NEMS. When a mass is added to a resonator, the mechanical resonance frequency is proportionally down-shifted. The degree of the frequency shift is used to determine the weight of the mass. Recently, significant progresses have improved the detection resolution of NEMS-based mass sensors to 1 yg.[11] It was demonstrated that NEMS resonators can be used as a single-particle detection sensor of a mass spectrometer.[12]

NEMS-based mass spectroscopy has drawn attention as an alternative approach to analyze biological systems.[13,14] It was particularly noted that NEMS resonators might be a promising tool for an emerging research field of single-molecule protein sequencing.[15−18] If the mass detection resolution reaches the order of several Daltons, it might be possible to distinguish different proteins or different proteoforms including isoforms from alternative splicing and post-translational modifications.[19] It is envisioned that, if such a high resolution is achieved at room temperature, NEMS-based mass spectroscopy can be widely used for applications. However, it is practically unlikely to implement a NEMS sensor that measures mass changes on the order of several Daltons at room temperature. The main difficulty is that when the temperature increases, the noise level of the resonance frequency of the NEMS resonator becomes very large due to thermal fluctuations.

Recently, an artificial-intelligence-based approach has been used for data analysis. This machine learning (ML) has been used in a wide range of applications such as voice search,[20] image recognition,[21] molecular/materials science,[22,23] and photonics devices.[24,25] It has demonstrated that ML can provide an efficient optimization and guidance for classification of scientific data.[22−25]

In this study, we used a convolutional neural network (CNN) learning-based applied ML technique for classification and estimated the limiting in mass detection of a suspended bilayer graphene-based nanomechanical resonator. This CNN learning-based approach allowed us to more quantitatively eliminate the thermal noise interferences and enable highly accurate mass detection. Noise pattern training by the ML algorithm can improve the accuracy of mass detection even when the noise level is comparable to or even higher than the signals from the mass change. Especially, 2D CNN can be

Received: May 11, 2022
Accepted: October 19, 2022
Published: October 27, 2022

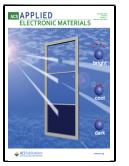

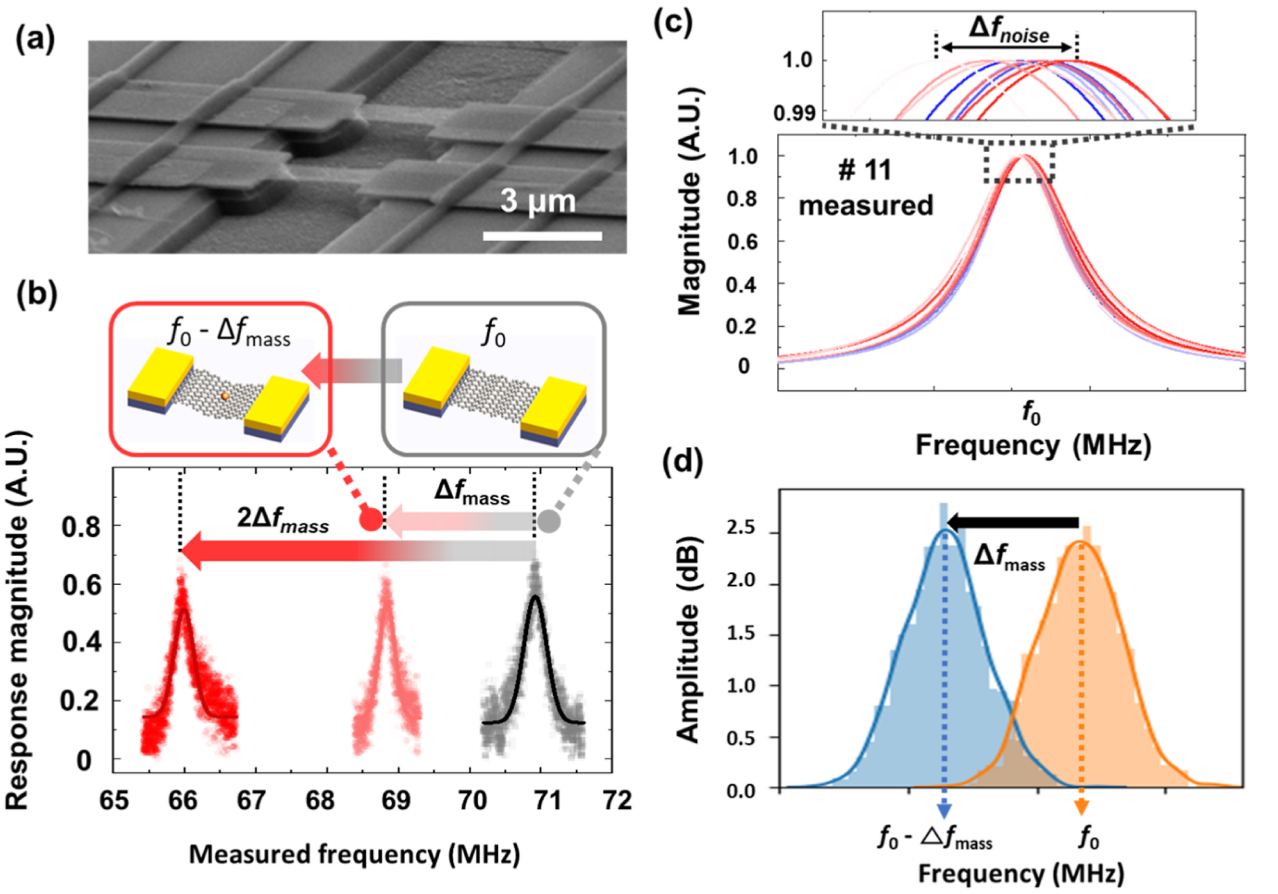

Figure 1. (a) SEM image of nanoresonators composed of suspended bilayer graphene. (b) Resonance frequencies of a suspended bilayer graphene resonator before and after depositing specific masses of Cr atoms (the above insets show the schematic of suspended bilayer devices before and after depositing Cr particles). (c) In situ 11 measurements without depositing a mass to estimate the thermal noise range in a bilayer graphene resonator. (d) Generated resonance frequency distributions based on Δf_{mass} and Δf_{noise}.

applied to the various data, and it is[26] a future-oriented technology. The 2D CNN can classify the mass change in real time using transfer learning that input data is adopted to pretrained model. Furthermore, we choose 1D CNN model because additional training on time-sequential data was also needed.

MATERIALS AND METHODS

Generation of a Resonance Frequency Distribution. As shown in a scanning electron microscopy (SEM) image (Figure 1a), we fabricated nanoresonators by suspending a bilayer graphene on a silicon substrate which was mounted on piezoelectric ceramic. The resonance frequency of the suspended bilayer graphene was measured using a 10 mW He−Ne laser with a wavelength of 633 nm and an AC voltage (1 V) applied to the piezoelectric ceramic in vacuum condition of 10^{-4} level. In this condition, the initial power of the laser is 10 mW, and the laser power output to the device is attenuated down to 0.1 mW in the detection process. The initial resonant frequency of the resonator without particles was 70.9 MHz, and then 1.6 and 3.2 fg of Cr particles were deposited,[27] the frequency shifted by 2 and 5 MHz (Δf_{mass} and $2\Delta f_{mass}$), respectively (Figure 1b). Figure 1c shows the initial resonant frequency obtained while measuring the resonator without mass, where a noise error range was attributable to thermal noise (white noise). There should be a lot of attributions, such as thermal fluctuation, structural deformation on the graphene device, oscillation on the circuits, and so forth, for generating errors on the resonance frequency of the graphene mechanical resonance device. In this simulation study, we focused on the thermal fluctuation-mediated error factor on the nanomechanical resonator since the device was operated at room temperature. The other noise factors could be removed or significantly reduced by improving the device fabrication procedure or measurement setup. However, the thermal excitation can be an inevitable error factor on detecting the mechanical resonance of a graphene device if we utilize this device for the mass detection sensor at room temperature. This is the reason why we especially focused on the thermal fluctuation-mediated error on the graphene mechanical resonator-based mass sensor. Here, the range of 11 measurement resonant frequencies is the drift level of thermal noise. The median value of the noise error range, Δf_{noise} = 68 kHz, was estimated from the repeated measurements. Data concerning arbitrary mass change was generated following a normal distribution and stored in a database based on the frequency shift caused by mass change (Δf_{mass}) and the noise error range caused by thermal noise (Δf_{noise}), as shown in Figure 1d.

Data Preprocessing and Feature Engineering: The Flow Chart for Learning and Classifying. A noise error owing to thermal noise or white noise always occurs in the bilayer graphene resonator. The noise is caused by the fluctuation of the molecules constituting the bilayer graphene and is thermal noise with a shift in mechanical frequency. Such noise obstructs an accurate mass detection using the resonator, making it essential to develop a technique capable of correcting it. For accurate and efficient mass detection against the effect of thermal noise, we used ML. Datasets were generated based on Gaussian distribution in which the measured shifts of resonance frequency due to the mass change (Δf_{mass}) and the noise range (Δf_{noise}) were combined as shown in Figure 2a. As shown in Figure 2b, the generated dataset consisted of 11 labels with different masses (0, Δf_{mass}, ..., $9\Delta f_{mass}$, and $10\Delta f_{mass}$), and feature engineering was performed in two methods based on this dataset. The

https://doi.org/10.1021/acsaelm.2c00628
ACS Appl. Electron. Mater. 2022, 4, 5184−5190

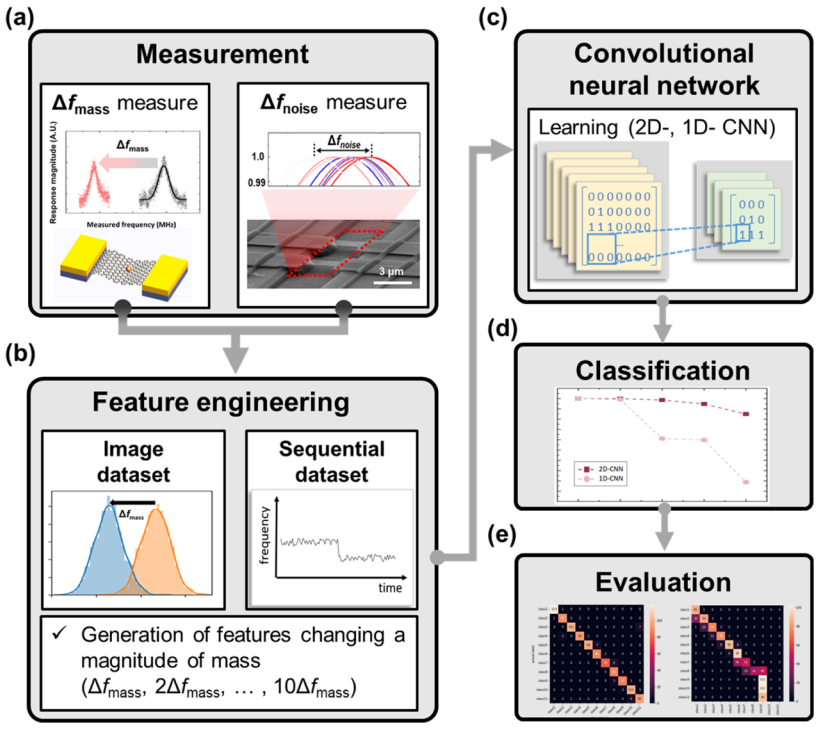

Figure 2. Flowchart for learning and classifying resonance frequencies with generated thermal noises. (a) Collecting the data of resonance frequencies and thermal noises in a bilayer graphene resonator. (b) Process of feature engineering the input data into image and sequential datasets based on the measured data. (c) Deep learning process with 2D and 1D CNNs. Steps of (d) classification and (e) evaluation.

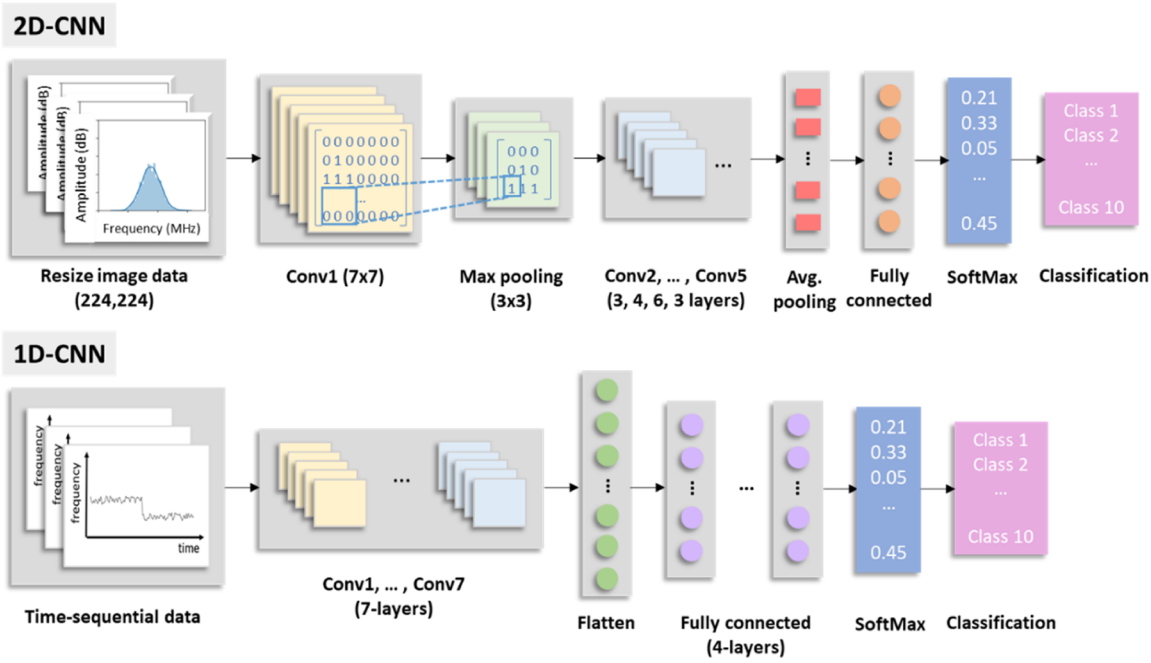

Figure 3. Detailed flowcharts of the 2D and 1D CNN algorithms.

sample size is 500−1000 per label, and labels of each dataset are incremented in multiples of the smallest unit of mass. If Δf_{mass} is $0.02\Delta f_{noise}$, label 1, label 2, label 3, label 4, and label 11 are Δf_{noise}, $0.02\Delta f_{noise}$, $0.04\Delta f_{noise}$, $0.06\Delta f_{noise}$, and $0.2\Delta f_{noise}$.

The first approach for featurization was to visualize a graph with frequency on the *x*-axis and amplitude on the *y*-axis, and the 11 labels were categorized as a function of resonance frequency shift from mass changes. The data corresponding to each label consisting of 1000 different graphs were combined with the thermal noise—within the estimated range as shown in Figure 1c—and the resonance frequency shift for a specific mass. The second approach for featurization was to produce time sequential data, in which the resonance frequency shifts when a mass is loaded at a specific time. In the first approach, the 11 labels were divided according to the mass change, and each was composed of 500 different time sequential data with thermal noise added. For cross-validation, the dataset was divided into a training set of 80% randomly selected and a test set with the remaining 20% before training the dataset. Then, as shown in Figure 2c, learning was performed using a CNN,[28] the first dataset consisting of image data was learned with 2D CNN,[29−31] and the time sequential dataset was

https://doi.org/10.1021/acsaelm.2c00628
ACS Appl. Electron. Mater. 2022, 4, 5184−5190

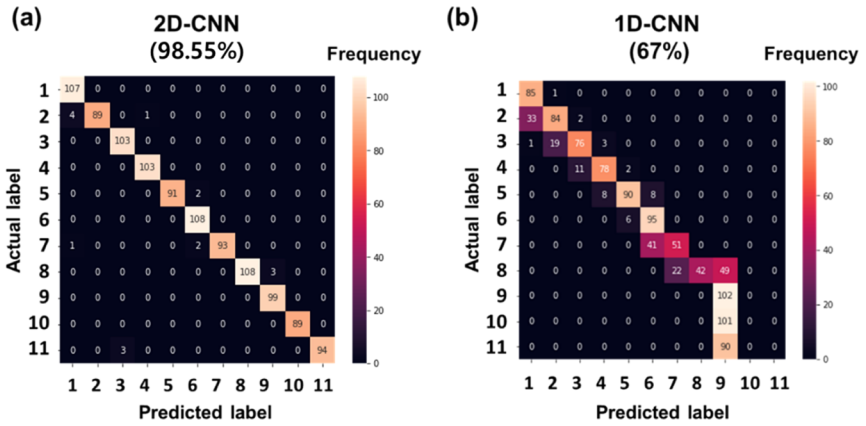

Figure 4. Confusion matrices for classification of 11 classes at a resonance frequency shift of 3.3% Δf_{noise} in (a) 2D CNN and (b) 1D CNN.

learned with 1D CNN.[32] The values learned through CNN were estimated as the probability for each label and classified as the specific label with the highest probability after 5-fold cross-validation as shown in Figure 2d. Consequently, such CNN learning-based classification was evaluated through the classification accuracy and also through the confusion matrix and f1-score in Figure 2e. Since simple classification accuracy is not high when data imbalance exists, classification accuracy was evaluated with the f1-score, which is the harmonic mean of precision and recall, and confusion matrix. Both precision and recall are related with the percentage of correct answer. Accurately, precision is the probability of actual correct answer among the predicted correct answer. Recall is the probability of predicted correct answer among the actual correct answer. f1-score can be checked through calculating the harmonic mean of precision and recall. If the data label is the correct answer but it is classified as the incorrect answer, it is false negative. If the data label is the incorrect answer but it is classified as the correct answer, it is called a false positive. In the confusion matrix, the remained parts are false negative and false positive except for true positive and true negative, indicating the accuracy score for each label.

The CNN learning-based classification discussed in the previous section was performed with 2D (image) and 1D (sequential) CNN depending on the configuration of the dataset as shown in Figure 3. First, in the case of 2D CNN, the input image with the fixed range of the x (frequency) and y (amplitude) axes is resized to 224 × 224. As shown in Figure S1, 112 × 112 and 300 × 300 resized images were also generated, learned, and classified, followed by estimating the training time and classification accuracy. (The accuracy and time increased as the resolution of the image increased, and the optimization in this study was performed based on the image of 224 × 224 size, considering the learning time). The resized image data passed through several convolution layers and pooling processes to extract features of pixels, and then the final score for each label was calculated through the softmax layer. The 1D CNN method was simpler than the 2D case, and features of one-dimensional data (frequency−time) were extracted through convolutional layer and flattening, and a score for each label was calculated through the softmax layer. Furthermore, the accuracy for classification and f1-score were obtained through 5-fold cross-validation[33] for both 2D and 1D CNNs. We also performed the hyperparameter tuning through changing conditions such as epoch and batch size to find optimal conditions.

RESULTS AND DISCUSSION

Classification Accuracy and Classifiable Limiting Mass. To estimate the classifiable limiting mass, learning and classification should be performed while changing the resonance frequency shift (Δf_{mass}), which defines the label.

Therefore, learning and classification processes were repeated by determining Δf_{mass} as a specific percentage (10, 5, 3.3, 2.5, and 2%) of the amplitude of the thermal noise range (Δf_{noise}). Figure 4 shows confusion matrices for classification of 11 classes (labels) at a resonance frequency shift of 3.3% amplitude of noise range ($\Delta f_{mass} = 0.033\Delta f_{noise}$) through both 2D and 1D CNNs. The confusion matrix of 1D CNN learning-based classification (sequential) in Figure 4b shows that the f1-score is as low as 0.67, and the actual label and predicted label do not match well with each other. In the case of 2D CNN learning-based classification (image) in Figure 4a, however, the f1-score is as high as 0.99, and the confusion matrix demonstrates a strong diagonal tendency, indicating that the predicted label correctly classifies the actual label (see Table S1).

Figure 5a shows confusion matrices for the classification of 11 classes in 2D CNN at resonance frequency shifts having 10, 5, 3.3, 2.5, and 2% of Δf_{noise}, respectively. The 2D CNN learning-based classification has a f1-score of 0.95 or more when $\Delta f_{mass} \geq 0.025\Delta f_{noise}$ as shown in Figure 5b and Table S1, indicating that the performance of this classification method is good enough to classify the correct label. When $\Delta f_{mass} = 0.02\Delta f_{noise}$, however, this method has an f1-score of 0.85, resulting in poor classification accuracy. We confirmed that the minimum resolution for the mass detection is $0.025\Delta f_{noise}$ when the 2D CNN approach was used. On the other hand, 1D CNN shows high classification performance with an f1-score of 0.99 when $\Delta f_{mass} \geq 0.05\Delta f_{noise}$ but has an f1-score of 0.61 or less when $\Delta f_{mass} < 0.05\Delta f_{noise}$, resulting in severe performance degradation.

CONCLUSIONS

We showed that the limit of mass change detection using the NEMS resonator-based mass sensor can be improved by using applied ML. A suspended bilayer graphene resonator was adapted as a model device for this study, and the resonance frequency shift according to the mass was used as the test dataset for analysis. By using CNN-based ML, we demonstrated the classifiable limiting mass in a bilayer graphene resonator. Featurization is divided into image and sequential datasets, and those datasets are trained and classified using 2D and 1D CNNs, respectively. The 2D CNN learning-based classification shows an excellent performance when $\Delta f_{mass} \geq 0.025\Delta f_{noise}$, and 1D CNN also shows a similar high performance when $\Delta f_{mass} \geq 0.05\Delta f_{noise}$. In conclusion, the combination of the suspended graphene resonator and applied ML is expected to enable more precise mass detection. Given that the state of the art of NEMS resonator mass detection

https://doi.org/10.1021/acsaelm.2c00628
ACS Appl. Electron. Mater. 2022, 4, 5184−5190

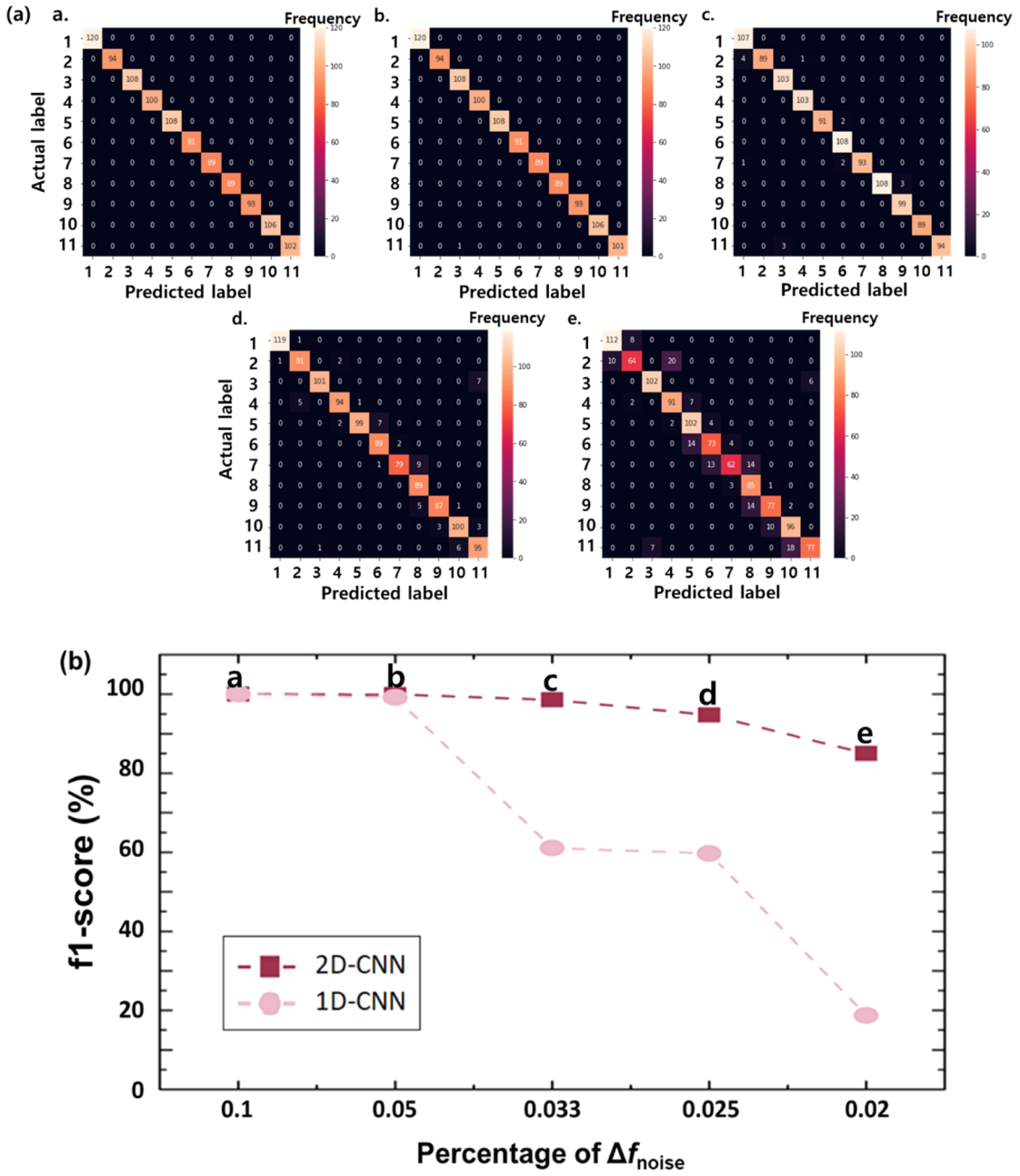

Figure 5. (a) Confusion matrices for the classification of 11 classes in 2D CNN and (b) f1-score accuracies of 2D and 1D CNNs at a resonance frequency shift of 10, 5, 3.3, 2.5, and 2% Δf_{noise}.

resolution is reported[9] around 100 Da level at room temperature, we expect that several Dalton of mass difference could be classified against noises by using our ML method. This work suggests the prospect of utilizing the NEMS resonator-based mass sensor for mass spectroscopy on the biomolecule detection including protein sequencing.

■ ASSOCIATED CONTENT

Supporting Information

The Supporting Information is available free of charge at https://pubs.acs.org/doi/10.1021/acsaelm.2c00628.

Accuracy and training time as a function of input image resolution; representative dataset for 1D and 2D CNN; and accuracy, precision, recall, and f1-score of 2D and 1D CNN learning based-classification (PDF)

■ AUTHOR INFORMATION

Corresponding Authors

Kookjin Lee − *Logic Technology Development Quality and Reliability, Intel Corporation, Hillsboro, Oregon 97124, United States;* orcid.org/0000-0002-9896-1090; Email: kookjin.lee@intel.com

Sang Wook Lee − *Department of Physics, Ewha Womans University, Seoul 03760, Republic of Korea;* orcid.org/0000-0003-2265-4761; Email: leesw@ewha.ac.kr

Authors

Miri Seo − *Department of Physics, Ewha Womans University, Seoul 03760, Republic of Korea*

Eunseo Yang − *Department of Physics, Ewha Womans University, Seoul 03760, Republic of Korea; Department of*

https://doi.org/10.1021/acsaelm.2c00628
ACS Appl. Electron. Mater. 2022, 4, 5184−5190

Computer Science and Engineering, Ewha Womans University, Seoul 03760, Republic of Korea

Dong Hoon Shin − *Kavli Institute of Nanoscience, Delft University of Technology, Delft 2628 CJ, The Netherlands*

Yugyeong Je − *Department of Physics, Ewha Womans University, Seoul 03760, Republic of Korea*

Chirlmin Joo − *Department of Physics, Ewha Womans University, Seoul 03760, Republic of Korea; Kavli Institute of Nanoscience, Delft University of Technology, Delft 2628 CJ, The Netherlands;* orcid.org/0000-0003-2803-0335

Complete contact information is available at: https://pubs.acs.org/10.1021/acsaelm.2c00628

Author Contributions

⊥M.S. and E.Y. contributed equally to this work.

Notes

The authors declare no competing financial interest.

We used Python libraries for generating the dataset and training/classifying the data (https://github.com/phys21/DeepMass).

■ ACKNOWLEDGMENTS

This research was supported by the Basic Research Program (NRF-2022R1A2B5B01001640 and NRF-2021R1A6A1A10039823) and the Global Research and Development Center Program (NRF-2018K1A4A3A01064272) through the National Research Foundation of Korea (NRF) and also supported by the Human Frontier Science Program (RGP00026/2019).

■ REFERENCES

(1) Ekinci, K. L.; Roukes, M. L. Nanoelectromechanical Systems. *Rev. Sci. Instrum.* **2005**, *76*, 061101.

(2) Schwab, K. C.; Roukes, M. L. Putting Mechanics into Quantum Mechanics. *Phys. Today* **2005**, *58*, 36−42.

(3) Teufel, J. D.; Donner, T.; Li, D.; Harlow, J. W.; Allman, M. S.; Cicak, K.; Sirois, A. J.; Whittaker, J. D.; Lehnert, K. W.; Simmonds, R. W. Sideband Cooling of Micromechanical Motion to the Quantum Ground State. *Nature* **2011**, *475*, 359−363.

(4) Palomaki, T. A.; Teufel, J. D.; Simmonds, R. W.; Lehnert, K. W. Entangling Mechanical Motion with Microwave Fields. *Science* **2013**, *342*, 710−713.

(5) Singh, V.; Bosman, S. J.; Schneider, B. H.; Blanter, Y. M.; Castellanos-Gomez, G. A.; Steele, G. A. Optomechanical Coupling between a Multilayer Graphene Mechanical Resonator and a Superconducting Microwave Cavity. *Nat. Nanotechnol.* **2014**, *9*, 820−824.

(6) Xu, Y.; Yan, S.; Jin, Z.; Wang, Y. Quantum-Squeezing Effects of Strained Multilayer Graphene NEMS. *Nanoscale Res. Lett.* **2011**, *6*, 355.

(7) Varshney, M.; Waggoner, P. S.; Tan, C. P.; Aubin, K.; Montagna, R. A.; Craighead, H. G. Prion Protein Detection Using Nanomechanical Resonator Arrays and Secondary Mass Labeling. *Anal. Chem.* **2008**, *80*, 2141−2148.

(8) Lassagne, B.; Garcia-Sanchez, D.; Aguasca, A.; Bachtold, A. Ultrasensitive Mass Sensing with a Nanotube Electromechanical Resonator. *Nano Lett.* **2008**, *8*, 3735−3738.

(9) Jensen, K.; Kim, K.; Zettl, A. An Atomic-Resolution Nanomechanical Mass Sensor. *Nat. Nanotechnol.* **2008**, *3*, 533−537.

(10) Ekinci, K. L.; Huang, X. M. H.; Roukes, M. L. Ultrasensitive Nanoelectromechanical Mass Detection. *Appl. Phys. Lett.* **2004**, *84*, 4469.

(11) Chaste, J.; Eichler, A.; Moser, J.; Ceballos, G.; Rurali, R.; Bachtold, A. A Nanomechanical Mass Sensor with Yoctogram Resolution. *Nat. Nanotechnol.* **2012**, *7*, 301−304.

(12) Sage, E.; Sansa, M.; Fostner, S.; Defoort, M.; Gély, M.; Naik, A. K.; Morel, R.; Duraffourg, L.; Roukes, M. L.; Alava, T.; Jourdan, G.; Colinet, E.; Masselon, C.; Brenac, A.; Hentz, S. Single-Particle Mass Spectrometry with Arrays of Frequency-Addressed Nanomechanical Resonators. *Nat. Commun.* **2018**, *9*, 3283.

(13) Rosłoń, I. E.; Japaridze, A.; Steeneken, P. G.; Dekker, C.; Alijani, F. Probing Nanomotion of Single Bacteria with Graphene Drums. *Nat. Nanotechnol.* **2022**, *17*, 637.

(14) Dominguez-Medina, S.; Fostner, S.; Defoort, M.; Sansa, M.; Stark, A. K.; Halim, M. A.; Vernhes, E.; Gely, M.; Jourdan, G.; Alava, T.; Boulanger, P.; Masselon, C.; Hentz, S. Neutral Mass Spectrometry of Virus Capsids above 100 Megadaltons with Nanomechanical Resonators. *Science* **2018**, *362*, 918−922.

(15) Restrepo-Pérez, L.; Joo, C.; Dekker, C. Paving the Way to Single-Molecule Protein Sequencing. *Nat. Nanotechnol.* **2018**, *13*, 786−796.

(16) Lill, J. R.; Mathews, W. R.; Rose, C. M.; Schirle, M. Proteomics in the Pharmaceutical and Biotechnology Industry: A Look to the next Decade. *Expert Rev. Proteomics* **2021**, *18*, 503−526.

(17) Timp, W.; Timp, G. Beyond Mass Spectrometry, the next Step in Proteomics. *Sci. Adv.* **2020**, *6*, 1−16.

(18) Callahan, N.; Tullman, J.; Kelman, Z.; Marino, J. Strategies for Development of a Next-Generation Protein Sequencing Platform. *Trends Biochem. Sci.* **2020**, *45*, 76−89.

(19) Alfaro, J. A.; Bohländer, P.; Dai, M.; Filius, M.; Howard, C. J.; van Kooten, X. F.; Ohayon, S.; Pomorski, A.; Schmid, S.; Aksimentiev, E.; Anslyn, C.; Bedran, G.; Cao, N.; Chinappi, R.; Coyaud, Z.; Dekker, S. H.; Dittmar, B.; Drachman, D.; Eelkema, S.; Goodlett, G.; Hentz, E. M.; Kalathiya, J. P.; Kelleher, C.; Kelly, M.; Kelman, P.; Kim, K.; Kuster, L.; Rodriguez-Larrea, D.; Lindsay, M.; Maglia, M.; Marcotte, P.; Marino, A.; Masselon, C.; Mayer, M.; Samaras, P.; Sarthak, K.; Sepiashvili, L.; Stein, D.; Wanunu, M.; Wilhelm, M.; Yin, P.; Meller, A.; Joo, C. The Emerging Landscape of Single-Molecule Protein Sequencing Technologies. *Nat. Methods* **2021**, *18*, 604−617.

(20) Vignal, C.; Mathevon, N.; Mottin, S. Audience Drives Male Songbird Response to Partner's Voice. *Nature* **2004**, *430*, 448−451.

(21) Lawrence, S.; Giles, C. L.; Ah Chung Tsoi, A. C.; Back, A. D. Face Recognition: A Convolutional Neural-Network Approach. *IEEE Trans. Neural Network.* **1997**, *8*, 98−113.

(22) Lee, K.; Nam, S.; Ji, H.; Choi, J.; Jin, J. E.; Kim, Y.; Na, J.; Ryu, M. Y.; Cho, Y. H.; Lee, H.; Lee, J.; Joo, M. K.; Kim, G. T. Multiple Machine Learning Approach to Characterize Two-Dimensional Nanoelectronic Devices via Featurization of Charge Fluctuation. *npj 2D Mater. Appl.* **2021**, *5*, 1−9.

(23) Lee, K.; Nam, S.; Kim, H.; Jeon, D. Y.; Shin, D.; Lim, H. G.; Kim, C.; Kim, D.; Kim, Y.; Byeon, S. H.; Kim, G. T. Detection and Accurate Classification of Mixed Gases Using Machine Learning with Impedance Data. *Adv. Theory Simul.* **2020**, *3*, 2000012.

(24) Patel, S. K.; Surve, J.; Katkar, V.; Parmar, J. Optimization of Metamaterial-Based Solar Energy Absorber for Enhancing Solar Thermal Energy Conversion Using Artificial Intelligence. *Adv. Theory Simul.* **2022**, *5*, 2200139.

(25) Patel, S. K.; Surve, J.; Katkar, V.; Parmar, J.; Al-Zahrani, F. A.; Ahmed, K.; Bui, F. M. Encoding and Tuning of THz Metasurface-Based Refractive Index Sensor With Behavior Prediction Using XGBoost Regressor. *IEEE Access* **2022**, *10*, 24797−24814.

(26) Kireeva, N.; Baskin, I. I.; Gaspar, H. A.; Horvath, D.; Marcou, G.; Varnek, A. Generative Topographic Mapping (GTM): Universal Tool for Data Visualization, Structure-Activity Modeling and Dataset Comparison. *Mol. Inform.* **2012**, *31*, 301−312.

(27) Kim, H.; Shin, D. H.; McAllister, K.; Seo, M.; Lee, S.; Kang, I.-S.; Park, B. H.; Campbell, E. E. B.; Lee, S. W. Accurate and Precise Determination of Mechanical Properties of Silicon Nitride Beam Nanoelectromechanical Devices. *ACS Appl. Mater. Interfaces* **2017**, *9*, 7282−7287.

(28) Kim, Y.Convolutional Neural Networks for Sentence Classification. *EMNLP 2014—Conference on Empirical Methods in Natural Language Processing (and Forerunners)*, 2014; pp 1746−1751.

(29) Zhengjun Pan, Z.; Rust, A. G.; Bolouri, H. Image Redundancy Reduction for Neural Network Classification Using Discrete Cosine Transforms. *Proc.—Int. Jt. Conf. Neural Networks* **2000**, *3*, 149−154.
(30) Masci, J.; Giusti, A.; Ciresan, D.; Fricout, G.; Schmidhuber, J.A Fast Learning Algorithm for Image Segmentation with Max-Pooling Convolutional Networks. *2022 IEEE International Conference on Image Processing*. ICIP 2013—Proc 20132013, 2013; pp 2713−2717.
(31) Nagi, J.; Ducatelle, F.; Di Caro, G. A.; Ciresan, D.; Meier, U.; Giusti, A.; Nagi, F.; Schmidhuber, J.; Gambardella, L. M.Max-Pooling Convolutional Neural Networks for Vision-Based Hand Gesture Recognition. *IEEE International Conference on Signal and Image Processing Applications (ICSIPA)*, 2011; pp 342−347.
(32) Zhao, J.; Mao, X.; Chen, L. Speech emotion recognition using deep 1D & 2D CNN LSTM networks. *Biomed. Signal Process Control* **2019**, *47*, 312−323.
(33) Schaffer, C. Selecting a classification method by cross-validation. *Mach. Learn.* **1993**, *13*, 135−143.

https://doi.org/10.1021/acsaelm.2c00628
ACS Appl. Electron. Mater. 2022, 4, 5184−5190